iScience

CellPress
OPEN ACCESS

Article

PGC-1α in the myofibers regulates the balance between myogenic and adipogenic progenitors affecting muscle regeneration

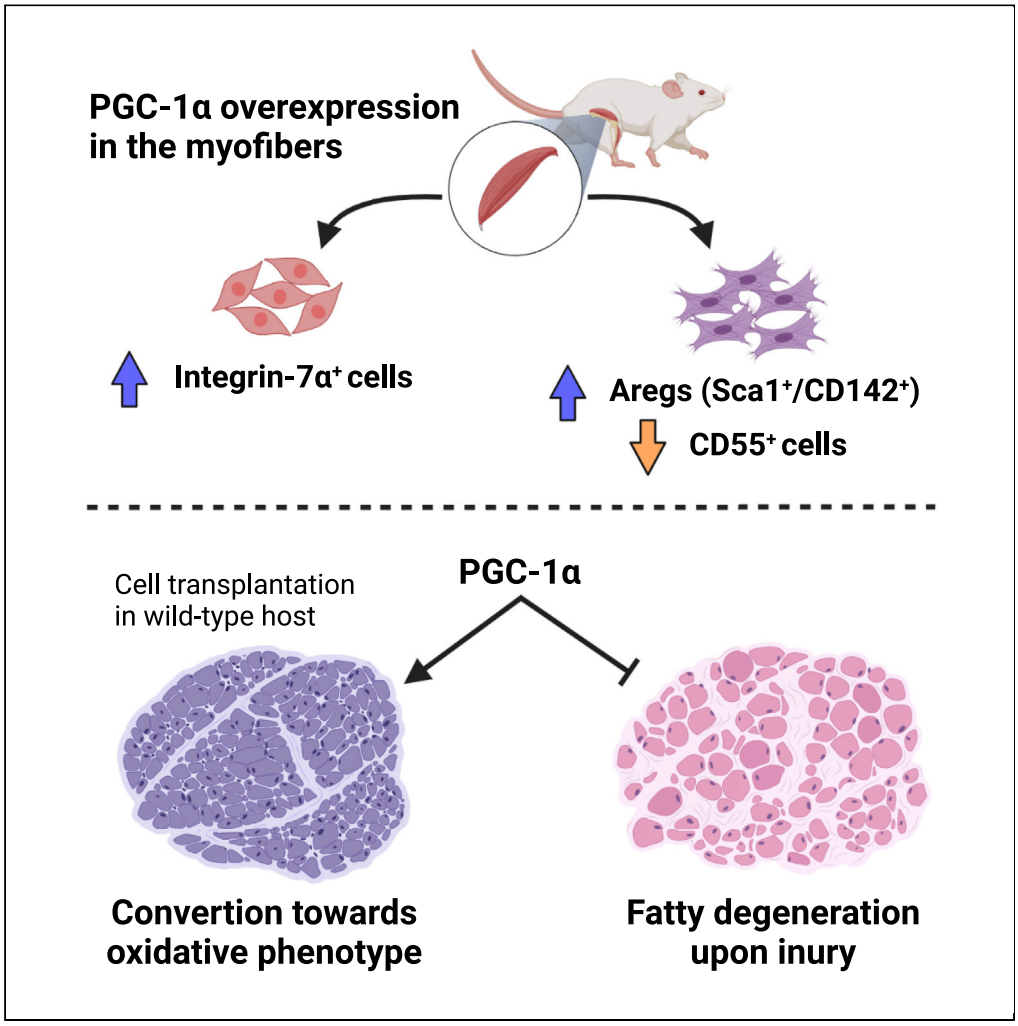

Marc Beltrà, Fabrizio Pin, Domiziana Costamagna, ..., Maurilio Sampaolesi, Fabio Penna, Paola Costelli

fabio.penna@unito.it (F.P.)
paola.costelli@unito.it (P.C.)

Highlights

Myofiber-specific PGC-1α overexpression alters the proportion of MuSCs and ISCs

Injection of MCK-PGC-1α cells promotes oxidative conversion of WT myofibers

MCK-PGC-1α mice are protected from intramuscular adipocyte accumulation

Beltrà et al., iScience 25, 105480
November 18, 2022
https://doi.org/10.1016/j.isci.2022.105480

iScience

CellPress
OPEN ACCESS

Article

PGC-1α in the myofibers regulates the balance between myogenic and adipogenic progenitors affecting muscle regeneration

Marc Beltrà,[1,2] Fabrizio Pin,[1,5] Domiziana Costamagna,[3] Robin Duelen,[3] Alessandra Renzini,[4] Riccardo Ballarò,[1,6] Lorena Garcia-Castillo,[1,2] Ambra Iannuzzi,[1] Viviana Moresi,[4] Dario Coletti,[4] Maurilio Sampaolesi,[3,4] Fabio Penna,[1,2,7,*] and Paola Costelli[1,2,7,8,*]

SUMMARY

Skeletal muscle repair is accomplished by satellite cells (MuSCs) in cooperation with interstitial stromal cells (ISCs), but the relationship between the function of these cells and the metabolic state of myofibers remains unclear. This study reports an altered proportion of MuSCs and ISCs (including adipogenesis-regulatory cells; Aregs) induced by the transgenic overexpression of peroxisome proliferator-activated receptor gamma coactivator 1-alpha (PGC-1α) in the myofibers (MCK-PGC-1α mice). Although PGC-1α–driven increase of MuSCs does not accelerate muscle regeneration, myogenic progenitors isolated from MCK-PGC-1α mice and transplanted into intact and regenerating muscles are more prone to fuse with recipient myofibers than those derived from wild-type donors. Moreover, both young and aged MCK-PGC-1α animals exhibit reduced perilipin-positive areas when challenged with an adipogenic stimulus, demonstrating low propensity to accumulate adipocytes within the muscle. Overall, these results unveil that increased PGC-1α expression in the myofibers favors pro-myogenic and anti-adipogenic cell populations in the skeletal muscle.

INTRODUCTION

Muscle regeneration is a complex multi-step process that relies on the satellite cells (MuSCs) responsible for the postnatal myogenesis and the maintenance of muscle integrity.[1] Under normal circumstances, MuSCs are quiescent and quickly activate on injury, dividing and differentiating into myoblasts, that ultimately fuse to generate new myofibers. Although muscle regeneration is dependent on MuSCs, it also requires the participation of other non-myogenic cells involved in orchestrating inflammation, debris clearance, extracellular matrix deposition and extrinsic regulation of MuSC activity.[2] In particular, interstitial stromal cells (ISCs) can participate to adult myogenesis and support MuSC function. The remarkable regenerative capacity of the skeletal muscle is compromised in aging because of decreased number and function of MuSCs, contributing to sarcopenia and frailty.[3–5] Age-related faulty muscle regeneration is partially attributed to the reduced ability of ISCs, in particular of fibro-adipogenic progenitors (FAPs), to support MuSC activation and differentiation.[6] Moreover, functional decline of accessory cell is characteristic of myopathies such as Duchenne muscular dystrophy and systemic conditions such as obesity, diabetes, and cancer cachexia.[7–11]

Mitochondria are critical for preserving the metabolic fitness of the skeletal muscle. These organelles are deeply interconnected and form a network regulated by dynamic processes involving mitochondrial biogenesis, fission, fusion and mitophagy.[12] On activation and differentiation, MuSCs undergo a major genetic reprogramming to become metabolically active. Shortly after exiting quiescence, mitochondrial genes are robustly induced and MuSCs quickly accumulate mitochondrial mass in order to support the increasing energy demand needed for cell proliferation and myotube formation.[13,14] Mitochondrial dysfunction is a distinctive aspect of MuSC senescence in aging.[15] Consistently, preventing the decline of mitochondrial metabolism during aging rescues MuSC myogenic potential,[15,16] demonstrating that mitochondria are essential for the functional maintenance of MuSCs. Among the known players contributing to mitochondrial homeostasis, the peroxisome proliferator-activated receptor gamma coactivator

[1]Experimental Medicine and Clinical Pathology Unit, Department of Clinical and Biological Sciences, University of Torino, Corso Raffaello 30, 10125 Turin, Italy

[2]Interuniversity Institute of Myology (IIM), 61029 Urbino, Italy

[3]Laboratory of Translational Cardiomyology, Department of Development and Regeneration, Stem Cell Research Institute, KU Leuven, 3000 Leuven, Belgium

[4]Unit of Histology and Medical Embryology, Department of Anatomy, Histology, Forensic Medicine and Orthopaedics, Sapienza University of Rome, 00161 Rome, Italy

[5]Present address: Department of Anatomy and Cell Biology, Indiana University School of Medicine, 46,202 Indianapolis IN, USA

[6]Present address: Department of Pediatrics, MD Anderson Cancer Center, 77,054 Houston TX, USA

[7]These authors contributed equally

[8]Lead contact

*Correspondence: fabio.penna@unito.it (F.P.), paola.costelli@unito.it (P.C.)

https://doi.org/10.1016/j.isci.2022.105480

1α (PGC-1α) stands out as powerful driver of mitochondrial biogenesis and regulator of processes such as mitochondria fusion-fission events and mitophagy.[17–22] Aside from promoting muscle oxidative metabolism, PGC-1α induces angiogenesis,[23] neuromuscular junction remodeling and increases the expression of structural proteins such as myosin heavy chain (MyHC) and utrophin.[24,25] Consistent with the broad effects on tissue plasticity, forced PGC-1α overexpression in several experimental models of atrophy preserves skeletal muscle function and myofiber morphology.[26–32]

In addition to its beneficial effects in the skeletal muscle, PGC-1α promotes the secretion of exercise-related myokines with both paracrine and endocrine functions, contributing to the crosstalk among muscle and fat, bone or brain.[33] Consistently, PGC-1α overexpression in mature myofibers impacts on the MuSC niche,[34] modulating the local pro- and anti-inflammatory cytokine balance.[35,36] Nonetheless, to our knowledge, no clear association exists between the predominant oxidative environment, as dictated by myofiber PGC-1α overexpression, and MuSC and ISC function. The present study provides cues on the indirect impact of PGC-1α in altering the balance and propensity to differentiate of myogenic and adipogenic populations that reside in the skeletal muscle.

RESULTS

PGC-1α expression is transiently induced in early phases of muscle regeneration

Muscle regeneration is a highly energy-demanding process, and a progressive increase of mitochondrial function occurs in order to respond to the increased energetic needs.[37] Along this line, we characterized the reprogramming of oxidative metabolism in the tibialis anterior (TA) muscle of wild-type (WT) mice after $BaCl_2$-induced injury. Muscle regeneration was assessed at 7, 10 and 13 days post injury (dpi), when new myofiber formation and maturation occurs, and at 49 dpi (7 weeks post-injury) as a final-phase myofiber maturation timepoint. Myofiber cross-sectional morphology was evidently disrupted at 7, 10 and 13 dpi, being associated with the presence of cell infiltrate, and was restored at 49 dpi, although central myonuclei still persisted (Figure 1A). Metabolic phenotype analysis, assessed succinate dehydrogenase (SDH) staining, revealed a lack of definite phenotype at 7 and 10 dpi, with apparent improvement at 13 dpi and complete recovery at 49 dpi (Figure 1B). This trend was consistent with the initial loss and the subsequent progressive restoration of mitochondrial SDHA protein levels as muscle regeneration proceeds (Figures 1C and 1D). Of interest, PGC-1α protein content was strongly increased at the initial stages of muscle regeneration (7 and 10 dpi), returning to normal levels at 13 and 49 dpi (Figures 1C and 1E). Consistently, expression of the PGC-1α downstream target gene *Cox4* was enhanced at 7 and 10 dpi (Figure 1F), although no changes in *Cycs* or *Sdha* expression was observed (Figures 1G and 1H). Notably, accumulation of PGC-1α protein levels correlated with the induction of myogenic markers *Pax7*, *Myog* and *Myh3,* and M1 macrophage marker *Cd68* at 7 and 10 dpi (Figures S1A–S1D). Regarding mitochondrial clearance, the mitophagy regulator gene *Prkn* was upregulated at 10 dpi (Figure 1I), whereas levels of *Fis1* and *Mfn2,* genes involved in mitochondrial fission and fusion respectably, remained unchanged (Figures 1J and 1K). Altogether, PGC-1α expression is induced as a consequence of myofiber formation and presumably promotes the expression of genes related to mitochondrial homeostasis during muscle regeneration.

PGC-1α-driven metabolic switch enhances myogenic potential of progenitor cell populations

The marked increase of PGC-1α in regenerating muscles paved the way to investigate whether modulating this transcriptional cofactor could impinge on myogenesis. To this aim, MCK-PGC-1α mice were used, which constitutively overexpress PGC-1α in adult skeletal muscle (Figure S2A). Beyond the elevated mitochondrial content (Figures S2B–S2D), MCK-PGC-1α mice show an increased absolute number of central myonuclei in TA muscle compared to WT mice in the absence of injury (Figure 2A), suggestive of ongoing regeneration. Consistent with this observation, enzymatic digestion of hindlimb muscles revealed a number of mononucleated cells in MCK-PGC-1α mice which was increased more than twice in comparison to WT animals (Figure 2B). In order to clarify if muscle-specific PGC-1α overexpression affected MuSC myogenic potential, myoblasts were isolated from two muscles with different metabolic phenotypes (the mostly glycolytic extensor digitorum longus (EDL), and the predominantly oxidative soleus) and cultured in differentiation medium. Myotubes differentiated from EDL-derived myoblasts of MCK-PGC-1α mice showed increased MyHC levels in comparison to those derived from WT-EDL. By contrast, myotubes obtained from soleus-derived myoblasts accumulated similar levels of MyHC, independently from mouse genotype (Figure 2C). These results indicate that the myofiber metabolic background likely influences the capacity of myogenic progenitors to generate fully differentiated myotubes *ex vivo*.

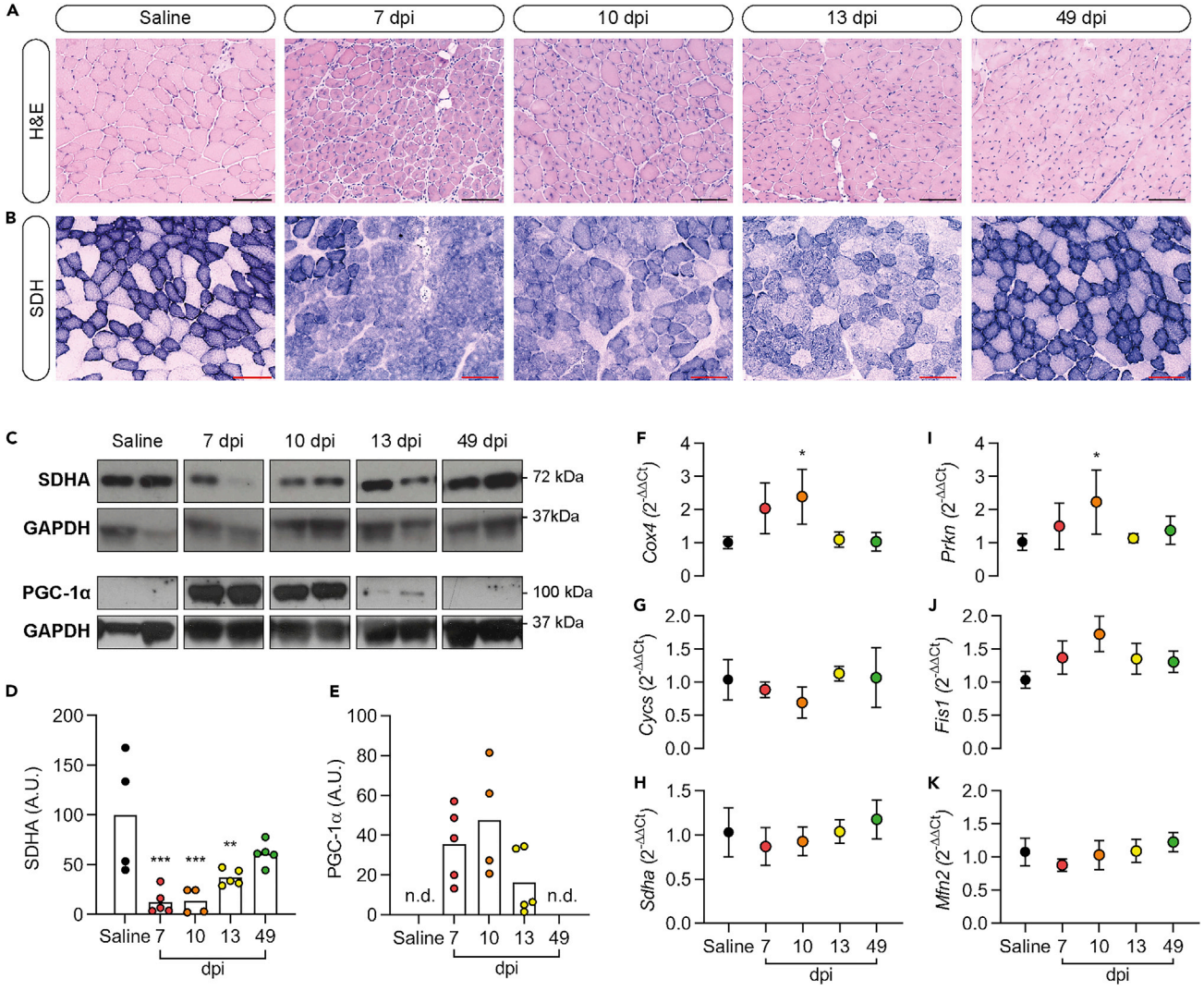

Figure 1. Modulation of mitochondrial markers during muscle regeneration

(A and B) Representative images of H&E and SDH staining of intact (saline) and $BaCl_2$-injected TA muscles (scale bar: 100 μm).

(C–E) Densitometry analysis of western blotting bands of SDHA and PGC-1α proteins. Total protein load was normalized by means of GAPDH protein expression.

(F–K) RT-qPCR quantification of *Cycs*, *Cox4*, *Sdha*, *Prkn*, *Fis1* and *Mfn2* genes. Data are normalized by *Actb* expression and displayed as relative expression ($2^{-\Delta\Delta Ct}$; mean ± SD) vs Saline group.

In panels (C–E) and (F–K), significance of the differences: *p<0.05, **p<0.01, ***p<0.001 vs Saline group (either One-way ANOVA+ Dunnett's test or Kruskal–Wallis + Dunn's test; n = 4-5 mice/group).

To better describe how PGC-1α overexpression impacts on myogenic populations, muscle interstitial cells were isolated, stained for integrin-α7 (a MuSC specific marker)[38] and characterized by flow cytometry (Figure S2E). The analysis revealed that the skeletal muscle of MCK-PGC-1α mice contains more integrin-$\alpha7^+$ cells in comparison to WT ones (Figure 2D). Next, the possibility of an artifactual overexpression of PGC-1α occurring in MuSCs was assessed. The results show that transcript levels of PGC-1α (*Ppargc1a*) and *Mck* were comparable in WT and MCK-PGC-1α-derived MuSCs grown in proliferating conditions (GM; Figure 2E), indicating that the transgene is not expressed. Indeed, should this occur, *Ppargc1a* and *Mck* mRNA levels would be higher in proliferating MCK-PGC-1α MuSCs than in WT ones. Consistently, after 3 days under differentiation conditions (DM), when *Mck is overexpressed,* higher levels of *Ppargc1a* were observed in MCK-PGC-1α-derived myotubes when compared to WT-derived ones (Figure 2E), likely in force of transgene transcription, which adds to the 'physiological' *Ppargc1a* mRNA levels.

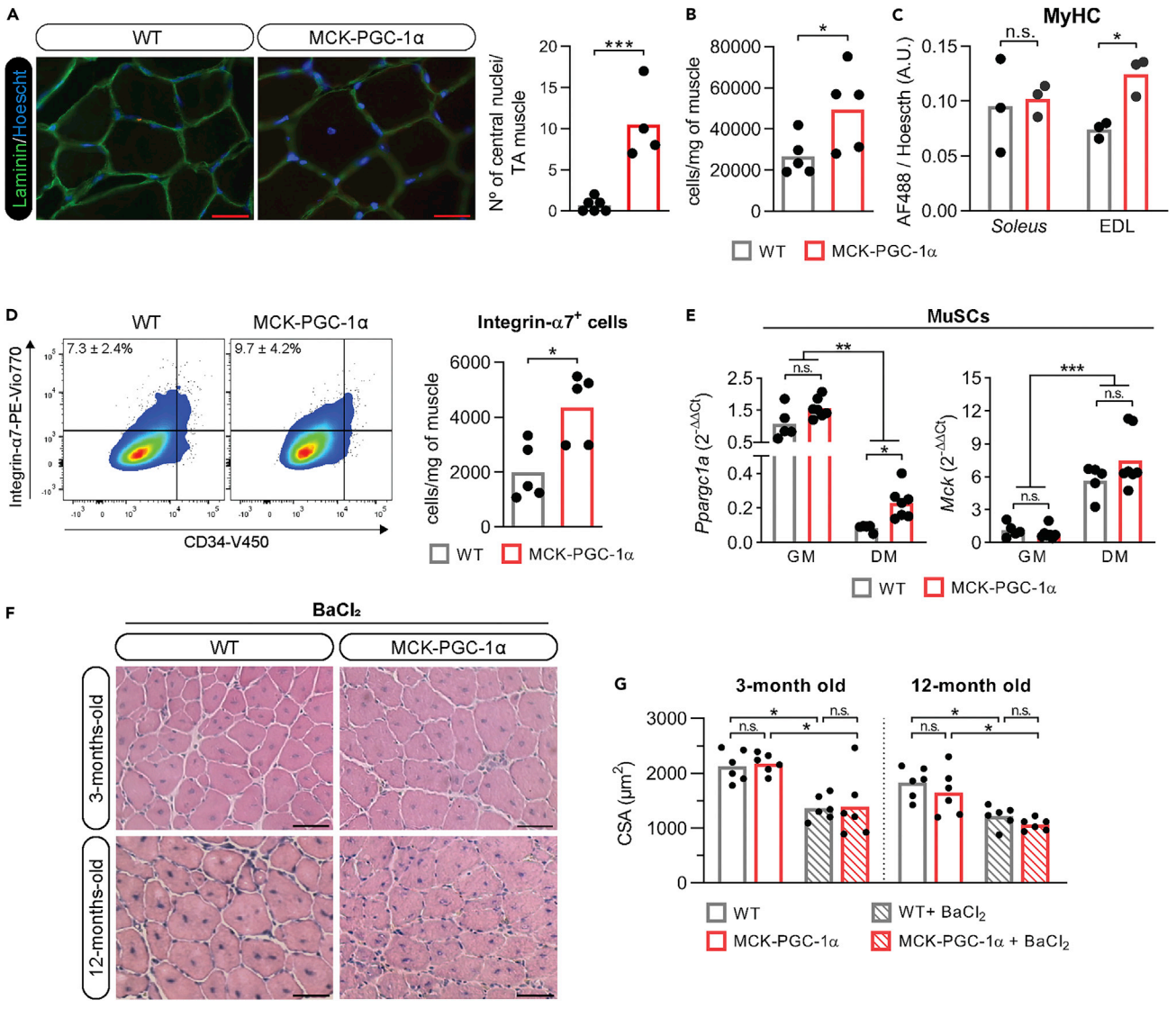

Figure 2. MCK-PGC-1α mice show increased myogenic precursors in the skeletal muscle, endowed with enhanced differentiation capacity *ex vivo* but not *in vivo*

(A) Representative images of Laminin/Hoechst immunostaining (scale bar: 25 μm) and quantification of central myonuclei of the whole area of a TA muscle section of WT and MCK-PGC-1α mice. ***p<0.001 (Student's *t* test; n = 6 WT mice, n = 4 MCK-PGC-1α mice).

(B) Total cell count after isolation of muscle interstitial cells from hindlimb muscles of WT and MCK-PGC-1α mice normalized per mg of tissue. Significance of the differences: *p<0.05 (Student's *t* test; n = 5 mice/group).

(C) Quantification of AF488 fluorescent signal according to anti-MyHC antibody binding in the supernatant of lysates of *soleus* and EDL-derived primary myotube cultures of both WT and MCK-PGC-1α mice. Significance of the differences: *p<0.05 (Student's *t* test; n = 3 mice/group).

(D) Representative panels of gate distribution and relative (referred to a cell sample of equal dimension) quantification of positive events (cells) according to anti-integrin-α7 and anti-CD34 antibody binding. Numbers in gates represent the percentage of cells (mean ± SD) by each specific labeling combination. Total number of integrin-α7$^+$ cells (bar plot) was obtained by normalizing integrin-α7 relative positivity to the number of isolated cells/mg of tissue (higher in MCK-PGC1α than in WT mice). Significance of the differences: *p<0.05 (Student's *t* test; n = 5 mice/group).

(E) *Ppargc1a* and *Mck* gene expression in proliferating (GM) and differentiated (DM) MuSCs derived from WT and MCK-PGC-1α cultured *ex vivo*. Data are normalized by *H2bc4* expression and displayed as relative expression ($2^{-\Delta\Delta Ct}$; mean). Significance of the differences: *p<0.05, **p<0.01, ***p<0.001 (Multiple Student's ttest corrected with Holm-Sidak method; n = 5 WT mice, n = 7 MCK-PGC-1α mice).

(F) Representative images of H&E staining (scale bar: 50 μm) of WT and MCK-PGC-1α mice injured using 1.2% $BaCl_2$ evaluated at 14 dpi.

(G) Myofiber cross-sectional area (CSA) of TA muscles expressed as percentage of WT intact muscles. Significance of the differences: **p<0.01 (two-way ANOVA+ Tukey's test; n = 6 mice/group).

Considering the accumulation of MuSCs in the skeletal muscle of transgenic animals, we tested if such abundance could result in improved muscle regeneration in middle-aged (12 months old) MCK-PGC-1α mice exposed to $BaCl_2$ injury. Basic histological analyses revealed neither macroscopic morphological changes nor improved myofiber cross-sectional area (CSA) in 3-month-old (young adult) transgenic animals compared to WT mice at 14 dpi (Figures 2F and 2G). Similarly, PGC-1α overexpression did not accelerate myofiber CSA recovery in middle-aged animals (Figures 2F and 2G). Overall, myofiber PGC-1α overexpression impacts on MuSC increasing their number and enhancing their *ex vivo* myogenic potential, being however unable to modulate the kinetic of injury-induced muscle regeneration.

Transplantation of MCK-PGC-1α-derived cells recapitulates the oxidative phenotype in the skeletal muscle of WT mice

Because constitutive PGC-1α overexpression did not impinge on *in vivo* regeneration, whereas MuSCs from MCK-PGC-1α mice displayed enhanced *ex vivo* myogenic capacity (Figure 2C), the possibility that transplantation of myogenic progenitors derived from transgenic animals could contribute to muscle regeneration *in vivo* was investigated. To this purpose, mononucleated cells were isolated from hindlimb muscles of WT and MCK-PGC-1α donor animals and injected into the skeletal muscle (injured or intact) of WT recipients, according to the protocol described in Figure 3A. At 14 dpi, muscles transplanted with WT cells no longer showed morphological evidence of ongoing regeneration (Figure 3B) and presented with fully recovered CSA and a similar number of myofibers to non-injured muscles (Figures 3C and 3D). Consistently, no alterations on myogenin (MyoG) protein content (Figure 3E) or *Myh3* gene expression (Figure S3) were observed. Nevertheless, Pax7 expression was increased in the injured group (Figure 3E), suggesting an increase in the MuSC pool. A completely different phenotype, with central myonuclei, cell infiltrate, reduced myofiber CSA and increased expression of Pax7 and MyoG was observed in both non-injured and injured muscles receiving MCK-PGC-1α cells (Figures 3B, 3C, and 3E). Moreover, an increased number of myofibers was reported in injured muscles on MCK-PGC-1α-derived cell injection (Figure 3D). This observation, associated with the parallel induction of *Myh3* expression (Figure S3), was suggestive of new myofiber formation. Regarding the mitochondrial status, injured muscles transplanted with WT cells showed a complete recovery of oxidative/glycolytic myofiber distribution (Figure 3F) together with the persistent accumulation of PGC-1α and COX-IV proteins (Figure 3G). Strikingly, intact muscles injected with MCK-PGC-1α cells (but not with WT cells) revealed a homogeneous SDH staining resembling the phenotype observed in transgenic animals (Figures 3F and S2B), suggesting that MCK-PGC-1α-derived myogenic progenitors might have fused into non-regenerating host myofibers, recapitulating the metabolic phenotype of transgenic mice. In addition, a similar metabolic conversion was observed in muscles injured before transplantation with transgenic cells (Figure 3F). Consistent with the hypothesis of transgenic myoblast fusion into host myofibers, PGC-1α and COX-IV protein levels increased in both uninjured and injured recipient muscles (Figure 3G). However, further studies are warranted to clearly demonstrate that transgenic myoblasts actually fuse with existing myofibers.

Overexpression of PGC-1α inhibits the adipogenic drift in the regenerating muscle

Muscle regeneration is not only dependent on MuSCs but also on ISCs. Deficient FAP function compromises MuSC activation, contributing to fibrosis and adipocyte infiltration during faulty muscle regeneration.[6,39] Recently, subpopulations of adipogenic regulators with the capacity of modulating adipogenesis have been identified in mammalian fat depots.[40,41] Moreover, cell populations with similar regulatory capabilities are found in the skeletal muscle as part of specific ISC subtypes.[42] To better investigate the effects of muscle-specific PGC-1α overexpression on both myogenic and non-myogenic cells, we isolated mononucleated cells from WT and MCK-PGC-1α muscles and analyzed the ISC distribution by flow cytometry. In comparison to WT mice, transgenic animals presented increased $Sca1^+$ cells associated with CD142 co-labeling, indicating an enrichment in adipogenesis regulators (Aregs; Figures 4A and 4B), a cell population described to exert anti-adipogenic functions.[40,42] On the contrary, the amounts of cells positive for CD55, a marker highly expressed in $DPP4^+$ pre-adipocytes,[41] was lower in MCK-PGC-1α mice than in WT animals (Figures 4A and 4C).

The altered proportions of Aregs and $CD55^+$ cells suggested that the propensity to accumulate adipocytes after injury was altered in the skeletal muscle of PGC-1α overexpressing animals. To this purpose, 50% glycerol (Gly) was injected in the TA muscle of young WT and MCK-PGC-1α mice, reproducing a muscle injury model that promotes adipogenic infiltration.[43] As expected, a regenerative-like phenotype (Figure 5A) and the induction of *Myh3* expression was observed in Gly-injected TA muscles (Figure 5B). Injured muscle

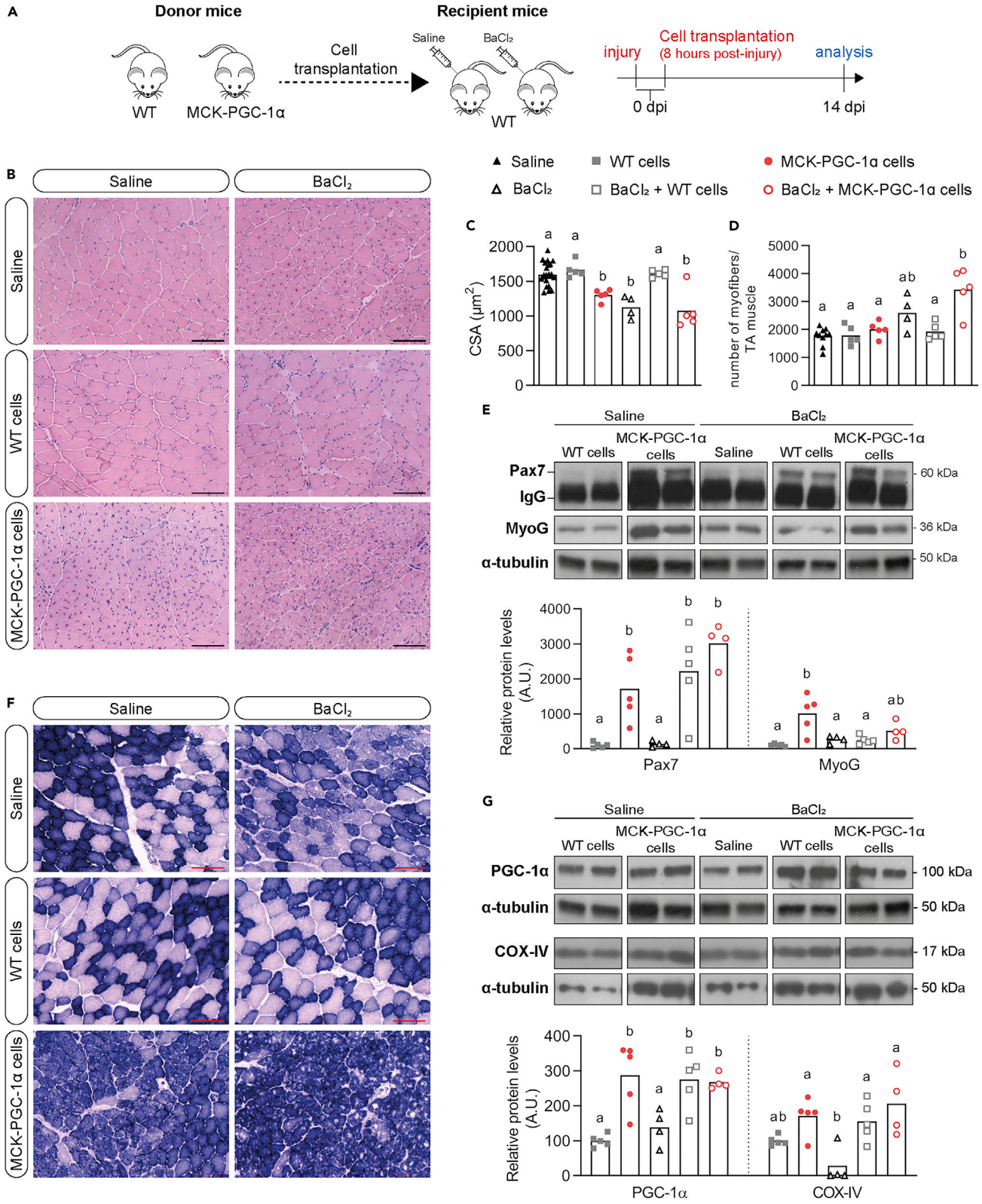
A
Donor mice
Recipient mice
WT
MCK-PGC-1α
Cell transplantation
Saline
BaCl₂
WT
injury
Cell transplantation
(8 hours post-injury)
analysis
0 dpi
14 dpi
B
Saline
BaCl₂
Saline
WT cells
MCK-PGC-1α cells
Saline
WT cells
MCK-PGC-1α cells
BaCl₂
BaCl₂ + WT cells
BaCl₂ + MCK-PGC-1α cells
C
CSA (μm²)
D
number of myofibers/ TA muscle
E
Saline
BaCl₂
WT cells
MCK-PGC-1α cells
Pax7
IgG
MyoG
α-tubulin
60 kDa
36 kDa
50 kDa
Relative protein levels (A.U.)
Pax7
MyoG
F
Saline
BaCl₂
G
PGC-1α
α-tubulin
COX-IV
100 kDa
50 kDa
17 kDa
PGC-1α
COX-IV

Figure 3. MCK-PGC-1α cell transplantation recapitulates the transgenic phenotype even in a non-regenerative environment

(A) Schematic representation of the transplantation experiment. Mononucleated cells were enzymatically isolated from hindlimb muscles of donor mice WT and MCK-PGC-1α mice and were transplanted to intact or injured TA muscles of recipient WT animals. Injured TA muscles were injected with 1.2% $BaCl_2$ approximately 8 h before cell transplantation and were sacrificed 14 dpi.

(B) Representative images of H&E staining (scale bar: 100 μm).

(C and D) CSA and total number of myofibers in a single TA muscle.

(E and G) Representative western blotting bands and densitometry analysis of Pax7, MyoG, PGC-1α and COX-IV proteins. Total protein load was normalized by means of α-tubulin protein expression. Pax7, MyoG and PGC-1α share the same α-tubulin normalization images because they were analyzed on the same gel.

(F) Representative images of SDH staining (scale bar: 100 μm).

In panels (C), (D), (E) and (G), groups with distinct letters are statistically different: $p<0.05$ (One-way ANOVA+ Tukey's test; n = 4-5 mice/group).

histology showed intramuscular white spots (Figure 5A), overlapping with Oil Red O (ORO) staining (Figure 5C). In addition, RT-qPCR analysis revealed that adipocyte-related genes *Plin1*, *Adipoq* and *Fadq4* were induced in the muscle of both WT and MCK-PGC-1α mice (Figure 5B), and perilipin immunofluorescence staining demonstrated the accumulation of intramuscular adipocytes (Figure 5D). Notably, expression of *Cd55* was significantly induced only in WT mice after Gly injury, whereas *Cd142* showed a strong tendency to increase in injured muscles of both WT and MCK-PGC-1α mice (Figure 5B). Consistent with the reported reduction in pre-adipocytes and increase in Aregs, adipocyte infiltration was partially prevented in MCK-PGC-1α animals as assessed by perilipin immunofluorescence and densitometric analysis of the perilipin positive area (Figure 5E), demonstrating blunted adipogenic differentiation in the skeletal muscle of transgenic animals.

To further investigate if muscle PGC-1α overexpression could reduce the adipogenic drift typically occurring during muscle regeneration in the elderly,[44,45] adipocyte infiltration in the skeletal muscle was also assessed in the above-mentioned 12-month-old WT and MCK-PGC-1α animals undergoing $BaCl_2$ injury (see data in Figures 2F and 2G). Perilipin-positive adipocytes were clearly detectable in injured muscles of middle-aged WT mice (Figure 5F). Consistent with the results obtained in young animals, older MCK-PGC-1α animals presented with a reduced accumulation of intramuscular adipocytes in comparison to WT ones (Figure 5G). The present results demonstrate that the predominant Areg subpopulation found in PGC-1α overexpressing muscles is associated with a decreased propensity to adipocyte differentiation during defective regeneration in aged animals.

DISCUSSION

Mounting evidence points to metabolism as a relevant factor in the regulation of stem cell quiescence, activation and differentiation in different tissues.[46] Specifically in the skeletal muscle, MuSC activation correlates with the induction of diverse metabolic pathways sustaining the high energy demand required for myoblast differentiation,[13] leading to an abrupt increase of mitochondrial activity and ATP availability.[14] In addition to supporting the increased energy demand, an increase in metabolic activity (both mitochondrial and non-mitochondrial) generates metabolites that impinge on intracellular pathways that regulate stem cell function.[47,48] The current work provides evidence that an early, potentially PGC-1α-driven, activation of mitochondrial biogenesis during muscle regeneration contributes to restore the metabolic phenotype of a healthy muscle (see Figure 1). The main novelty is the qualitative and quantitative impact exerted by myofiber-overexpressed PGC-1α on the different muscle stem cell populations, including MuSCs and ISCs.

In the experimental conditions adopted in the current study, muscle regeneration occurred with comparable kinetic in WT and MCK-PGC-1α animals, which does not properly fit with the enhanced *ex vivo* differentiation capacity of EDL-derived myogenic progenitor cells. In this regard, PGC-1α effects on myogenesis *in vivo* could be amplified in conditions characterized by disrupted muscle regeneration such as muscular dystrophies, whereas in healthy conditions the availability of more MuSCs might not impact on an already efficient regeneration process. The other way around, syngeneic allograft of transgenic muscle-derived cells recapitulated the oxidative phenotype in both injured and intact recipient muscles. Considering that exogenous cell engraftment is rarely observed in the absence of host muscle damage,[49] the oxidative conversion observed in uninjured muscles supports the possibility that transgenic cells likely have increased fusion capability and myogenic potential. A suggestive speculation in this regard is that the metabolically oxidative environment in the muscle of origin might predispose transgenic MuSCs with an increased ability to fuse, even in the absence of a regenerative stimulus. The high MyoG expression

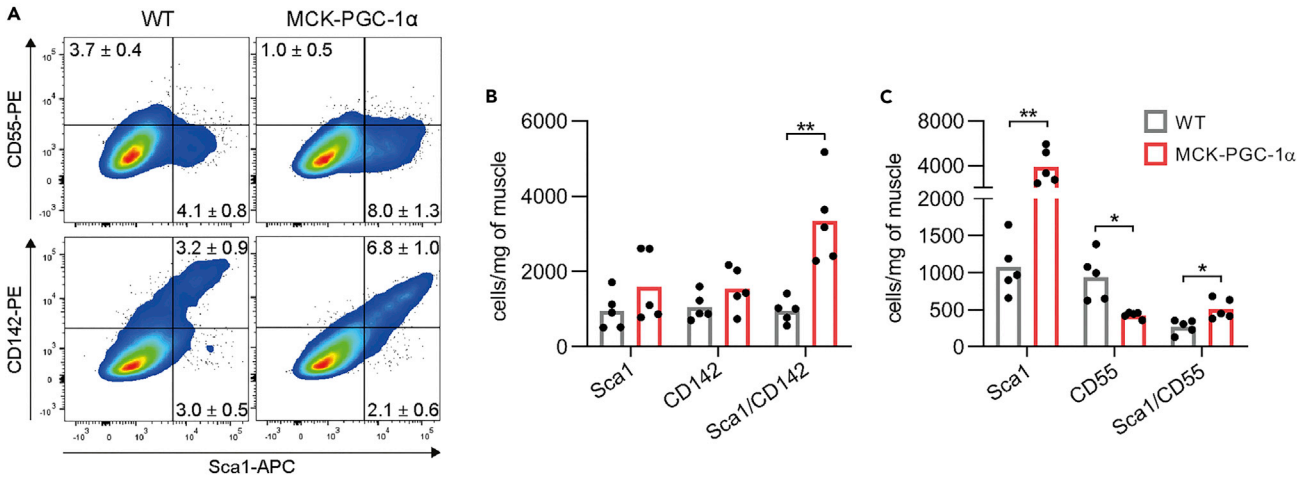

Figure 4. PGC-1α promotes the accumulation of Aregs against pre-adipocytes in the skeletal muscle

(A) Representative panel of gate distribution and relative quantification of positive events (cells) according to anti-Sca1, anti-CD55 or anti-CD142 antibody binding. Numbers in gates represent the percentage of cells (mean ± SD) by each specific labeling combination.

(B) Sca1+, CD142+ and Sca1+/CD142+ cells normalized by total number of isolated cells by mg of tissue.

(C) Sca1+, $CD55^+$ and Sca1+/CD55+ cells normalized by total number of isolated cells by mg of tissue.

In panels (B) and (C), significance of the differences: *p<0.05, **p<0.01 vs WT group (Student's *t* test; n = 5 mice/group).

in muscles transplanted with MCK-PGC-1α-derived cells could partially explain the increased fusion potential, consistently with recent evidence highlighting a central role played by MyoG in myoblast fusion.[50] However, the exact mechanism accounting for the improved ability of transgenic muscle progenitors to differentiate and fuse is far from being elucidated.

The present study also shows for the first time that myofiber PGC-1α overexpression prevents intramuscular fat accumulation. Intramuscular adipogenesis consequent to glycerol exposure is associated with an exacerbated inflammatory response as compared to the cardiotoxin-induced injury, with the activation of adipogenic regulatory networks and with reduction of fatty acid β-oxidation.[51] Data obtained in mice carrying a PDGFRα-reporter transgene indicate that most of the adipocytes that accumulate after glycerol injury arise from mesenchymal progenitors called FAPs.[39] However, whether FAPs can independently differentiate to adipocytes or require the interaction with other interstitial cells is still debated. The implementation of single cell transcriptomics to muscle regeneration has revealed that the $Sca1^+$/$PDGFR\alpha^+$ cell pool includes a peculiar $CD142^+$ population (Aregs) able to interfere with the propensity of $CD142^-$ ISCs to undergo adipogenic differentiation.[42] The present study shows that the decreased accumulation of mature adipocytes occurring in the muscle of MCK-PGC-1α animals correlates with am unbalance between Aregs and $CD55^+$ cells, the former being more abundant than the latter. These results are in line with previous observations demonstrating a regulatory role of Aregs on adipocyte differentiation and support the idea that the adipogenic fate of mesenchymal progenitors is modulated by the balance of specific ISCs populations that reside in the extracellular matrix.[40,42]

From a mechanistic point of view, it is conceivable that PGC-1α action on MuSCs and ISCs is driven by paracrine factors secreted by PGC-1α-overexpressing myofibers.[33] MCK-PGC-1α mice display high irisin levels, a polypeptide able to promote browning of the white adipose tissue,[52] thus being a factor potentially affecting adipocyte differentiation. Other hormonal mediators involved in modulating ISCs mitochondrial bioenergetics could also contribute to the anti-adipogenic drive reported in Gly-injured muscle of MCK-PGC-1α animals. For instance, impaired muscle regeneration and increased muscle adiposity induced by the genetic inhibition of α-Klotho mainly results from mitochondrial dysfunction in activated MuSCs.[53] This report could be consistent with the observation that in MCK-PGC-1α animals, characterized by a pro-oxidative muscle metabolic phenotype, adipogenic differentiation after glycerol injury or in $BaCl_2$-treated middle-aged mice is inhibited.

The inhibition of adipogenesis in MCK-PGC-1α animals is particularly relevant to the study of diseases characterized by the progressive substitution of muscle mass with ectopic fat. Consistently, the results

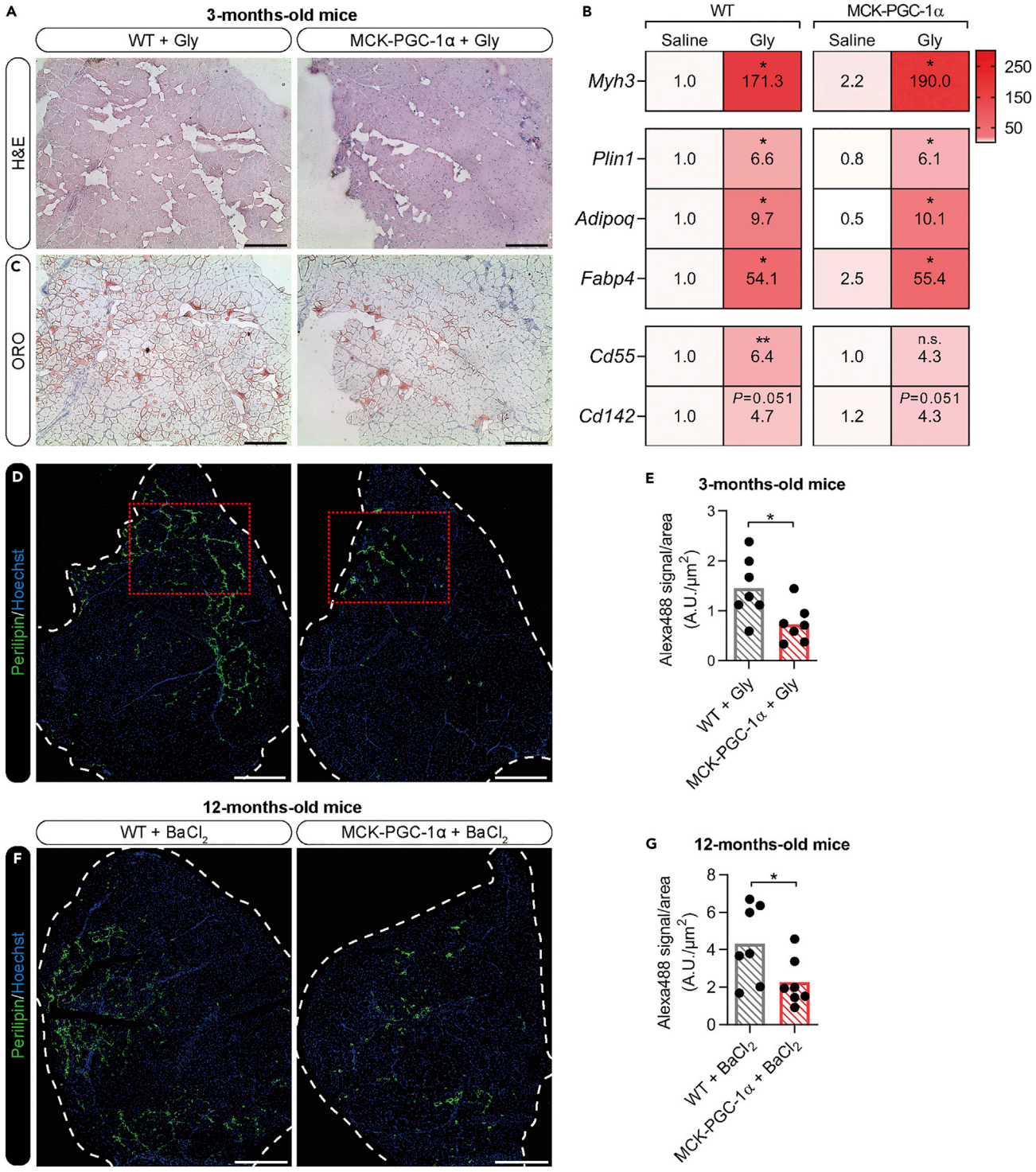

Figure 5. Muscle PGC-1α overexpression prevents the accumulation of intramuscular adipocytes

(A) Representative images of H&E staining (scale bar: 200 μm).

(B) Heatmap showing relative expression of *Myh3*, *Plin1*, *Adipoq*, *Fapb4*, *Cd55* and *Cd142* genes by RT-qPCR quantification of 3-month-old WT and MCK-PGC-1α mice injected with 50% glycerol (Gly) at 21 dpi. Data are normalized by *Actb* expression and displayed as relative expression ($2^{-\Delta\Delta Ct}$; mean) vs WT-Sham group. Significance of the differences: *p<0.05 vs WT-Sham or MCK-PGC-1α-Sham group (two-way ANOVA+ Holm-Šídák test; n = 7 mice/group).

(C) Representative images of ORO staining (scale bar: 200 μm).

Figure 5. *Continued*

(D and F) Representative images of perilipin/Hoechst immunostaining of TA muscle (scale bar: 500 μm) of (D) 3-month-old WT and MCK-PGC-1α mice injected with Gly at 21 dpi and (F) 12-month-old WT and MCK-PGC-1α mice injected with $BaCl_2$ at 14 dpi. White dotted lines indicate the boarders of the TA muscle. In D, red-doted rectangles highlight the same area shown in panels A and C.

(E and G) Densitometric quantification of Alexa488 signal, proportional to anti-perilipin antibody labeling. Significance of the differences: *p<0.05 (Student's *t* test; n = 7 mice/group).

reported here reveal that adipocyte accumulation occurs in the injured muscle of middle-aged animals, and that such adipogenic drift is partially hindered in age-matched PGC-1α-overexpressing mice, entailing a promising connection between ISC dysfunction in aging and muscle oxidative metabolism. To fully validate these observations, further research should be performed on old and geriatric animals, as lipodystrophy occurring after regeneration increases with age and negatively affects muscle function.[44,45] In addition, clarifying the mechanisms underlying the regulatory function exerted by PGC-1α on adipogenic populations is highly relevant to chronic muscle pathologies such as Duchenne muscular dystrophy or limb girdle muscular dystrophy 2B. Such diseases, indeed, are characterized by poor muscle morphology and increased disease severity that are associated with progressive replacement of muscle tissue with fat.[54,55]

In conclusion, the current results propose PGC-1α as a modulator of MuSCs and ISCs in the skeletal muscle, favoring the myogenic lineage over the adipogenic one. Overall, the data reported here support the idea that harnessing muscle metabolism could become a therapeutic tool to treat muscle conditions characterized by impaired muscle regeneration.

Limitations of the study

The PGC-1α transgenic construct used for this study is under the control of the MCK promoter,[56] implying that only mature myofibers overexpress PGC-1α in intact skeletal muscle. However, MyoD was shown to bind and activate the MCK promoter.[57] Although the present study shows that MuSCs in growing culture conditions obtained from transgenic animals do not present with overexpression of PGC-1α, we cannot rule out that the isolation procedure, involving MuSC removal from their niche and the consequent rapid induction of MyoD,[58] could result in a transient PGC-1α transgene induction critical to enhance progenitor cell engraftment because promotion of mitochondrial respiration in myogenic progenitors was proven sufficient to endorse their differentiation potential.[59] In this line, a hypothetical early overexpression of PGC-1α in myogenic precursor cells could increase mitochondrial content in MuSCs, and would therefore partially recapitulate the increased differentiation capability observed in human myoblasts by Haralampieva et al.[60] Furthermore, and despite published evidence supporting the above hypothesis implying that PGC-1α action on MuSCs and ISCs might occur through paracrine mechanisms, the present study does not offer results on transgenic myofiber secretome, a limitation that deserves to be overcome in future studies.

STAR★METHODS

Detailed methods are provided in the online version of this paper and include the following:

- KEY RESOURCES TABLE
- RESOURCE AVAILABILITY
  - Lead contact
  - Material availability
  - Data and code availability
- EXPERIMENTAL MODEL AND SUBJECT DETAILS
  - Animal housing and ethics
  - Mouse models and experimental design
  - Organ culture
  - MuSCs isolation, culture and differentiation
- METHOD DETAILS
  - Myosin quantification
  - Whole muscle cell isolation, transplantation and flow cytometric analysis
  - Muscle histology
  - Isolation, retro-transcription and RT-qPCR quantification of mRNA

SUPPLEMENTAL INFORMATION

Supplemental information can be found online at https://doi.org/10.1016/j.isci.2022.105480.

ACKNOWLEDGMENTS

This work was supported by World Anti-Doping Agency (WADA; Grant IOC15E01PC, P.I. P. Costelli), Fondazione Cariplo (Grant 2017-0604 to F. Penna), Fondazione AIRC (IG 2018—ID. 21963 project, P.I. F. Penna), University of Torino (ex-60% funds), Consorzio Interuniversitario Biotecnologie (Contributi mobilità 2018 to M. Beltrà), Association Française contre les Myopathies (AFM)-Téléthon (European Post-doctoral fellowship n°20673; to D. Costamagna) and Fonds Wetenschappelijk Onderzoek (FWO; Grant G0D4517N to M. Sampaolesi). The graphical abstract was created with BioRender.com.

AUTHOR CONTRIBUTIONS

Conceptualization, M.B., F. Pe., and P.C.; Investigation, M.B., F. Pi, D. Cos., R.D., A.R., R.B., L.G-C., and A.I.; Writing – Original Draft, M.B., F. Pe., and P.C.; Writing – Review & Editing, D. Cos., R.D., V.M., D. Col., and M.S.; Funding Acquisition, M.B., D. Cos., M.S., F. Pe., and P.C; Supervision, M.S., F. Pe., and P.C.

DECLARATION OF INTERESTS

The authors declare no competing interests.

INCLUSION AND DIVERSITY

We support inclusive, diverse, and equitable conduct of research.

Received: April 7, 2022
Revised: September 30, 2022
Accepted: October 28, 2022
Published: November 18, 2022

REFERENCES

1. Collins, C.A., Olsen, I., Zammit, P.S., Heslop, L., Petrie, A., Partridge, T.A., and Morgan, J.E. (2005). Stem cell function, self-renewal, and behavioral heterogeneity of cells from the adult muscle satellite cell niche. Cell *122*, 289–301. https://doi.org/10.1016/j.cell.2005.05.010.

2. Wosczyna, M.N., and Rando, T.A. (2018). A muscle stem cell support group: coordinated cellular responses in muscle regeneration. Dev. Cell *46*, 135–143. https://doi.org/10.1016/j.devcel.2018.06.018.

3. Sousa-Victor, P., Gutarra, S., García-Prat, L., Rodriguez-Ubreva, J., Ortet, L., Ruiz-Bonilla, V., Jardí, M., Ballestar, E., González, S., Serrano, A.L., et al. (2014). Geriatric muscle stem cells switch reversible quiescence into senescence. Nature *506*, 316–321. https://doi.org/10.1038/nature13013.

4. Liu, W., Klose, A., Forman, S., Paris, N.D., Wei-LaPierre, L., Cortés-Lopéz, M., Tan, A., Flaherty, M., Miura, P., Dirksen, R.T., et al. (2017). Loss of adult skeletal muscle stem cells drives age-related neuromuscular junction degeneration. Elife *6*, 1–15. https://doi.org/10.7554/eLife.26464.

5. Liu, L., Charville, G.W., Cheung, T.H., Yoo, B., Santos, P.J., Schroeder, M., and Rando, T.A. (2018). Impaired notch signaling leads to a decrease in p53 activity and mitotic catastrophe in aged muscle stem cells. Cell Stem Cell *23*, 544–556.e4. https://doi.org/10.1016/j.stem.2018.08.019.

6. Lukjanenko, L., Karaz, S., Stuelsatz, P., Gurriaran-Rodriguez, U., Michaud, J., Dammone, G., Sizzano, F., Mashinchian, O., Ancel, S., Migliavacca, E., et al. (2019). Aging disrupts muscle stem cell function by impairing matricellular WISP1 secretion from fibro-adipogenic progenitors. Cell Stem Cell *24*, 433–446.e7. https://doi.org/10.1016/j.stem.2018.12.014.

7. Verhaart, I.E.C., and Aartsma-Rus, A. (2019). Therapeutic developments for Duchenne muscular dystrophy. Nat. Rev. Neurol. *15*, 373–386. https://doi.org/10.1038/s41582-019-0203-3.

8. Penna, F., Costamagna, D., Fanzani, A., Bonelli, G., Baccino, F.M., and Costelli, P. (2010). Muscle wasting and impaired myogenesis in tumor bearing mice are prevented by ERK inhibition. PLoS One *5*, e13604. https://doi.org/10.1371/journal.pone.0013604.

9. Fu, X., Zhu, M., Zhang, S., Foretz, M., Viollet, B., and Du, M. (2015). Obesity impairs skeletal muscle regeneration via inhibition of AMP-activated protein kinase. Diabetes *65*, db150647. https://doi.org/10.2337/db15-0647.

10. Inaba, S., Hinohara, A., Tachibana, M., Tsujikawa, K., and Fukada, S. (2018). Muscle regeneration is disrupted by cancer cachexia without loss of muscle stem cell potential. PLoS One *13*, e0205467. https://doi.org/10.1371/journal.pone.0205467.

11. Costamagna, D., Duelen, R., Penna, F., Neumann, D., Costelli, P., and Sampaolesi, M. (2020). Interleukin-4 administration improves muscle function, adult myogenesis, and lifespan of colon carcinoma-bearing mice. J. Cachexia. Sarcopenia Muscle, jcsm. *11*, 783–801. https://doi.org/10.1002/jcsm.12539.

12. Hood, D.A., Memme, J.M., Oliveira, A.N., and Triolo, M. (2019). Maintenance of skeletal muscle mitochondria in Health, exercise, and aging. Annu. Rev. Physiol. *81*, 19–41. https://doi.org/10.1146/annurev-physiol-020518-114310.

13. Dell'Orso, S., Juan, A.H., Ko, K., Naz, F., Gutierrez-Cruz, G., Feng, X., and Sartorelli, V. (2019). Single-cell analysis of adult skeletal muscle stem cells in homeostatic and regenerative conditions. Development *146*, dev181743. https://doi.org/10.1242/dev.174177.

14. Tang, A.H., and Rando, T.A. (2014). Induction of autophagy supports the bioenergetic demands of quiescent muscle stem cell activation. EMBO J. *33*, 2782–2797. https://doi.org/10.15252/embj.201488278.

15. Zhang, H., Ryu, D., Wu, Y., Gariani, K., Wang, X., Luan, P., D'Amico, D., Ropelle, E.R., Lutolf, M.P., Aebersold, R., et al. (2016). NAD^+ repletion improves mitochondrial and stem cell function and enhances life span in mice. Science *352*, 1436–1443. https://doi.org/10.1126/science.aaf2693.

16. Brett, J.O., Arjona, M., Ikeda, M., Quarta, M., de Morrée, A., Egner, I.M., Perandini, L.A., Ishak, H.D., Goshayeshi, A., Benjamin, D.I., et al. (2020). Exercise rejuvenates quiescent skeletal muscle stem cells in old mice through restoration of Cyclin D1. Nat. Metab. *2*, 307–317. https://doi.org/10.1038/s42255-020-0190-0.

17. Wu, Z., Puigserver, P., Andersson, U., Zhang, C., Adelmant, G., Mootha, V., Troy, A., Cinti, S., Lowell, B., Scarpulla, R.C., et al. (1999). Mechanisms controlling mitochondrial biogenesis and respiration through the thermogenic coactivator PGC-1. Cell *98*, 115–124. https://doi.org/10.1016/S0092-8674(00)80611-X.

18. Soriano, F.X., Liesa, M., Bach, D., Chan, D.C., Palacin, M., and Zorzano, A. (2006). Evidence for a mitochondrial regulatory pathway defined by peroxisome proliferator-activated receptor- coactivator-1 , estrogen-related receptor- , and mitofusin 2. Diabetes *55*, 1783–1791. https://doi.org/10.2337/db05-0509.

19. Vainshtein, A., Desjardins, E.M., Armani, A., Sandri, M., and Hood, D.A. (2015). PGC-1α modulates denervation-induced mitophagy in skeletal muscle. Skelet. Muscle *5*, 9. https://doi.org/10.1186/s13395-015-0033-y.

20. Halling, J.F., Ringholm, S., Olesen, J., Prats, C., and Pilegaard, H. (2017). Exercise training protects against aging-induced mitochondrial fragmentation in mouse skeletal muscle in a PGC-1α dependent manner. Exp. Gerontol. *96*, 1–6. https://doi.org/10.1016/j.exger.2017.05.020.

21. Yeo, D., Kang, C., Gomez-Cabrera, M.C., Vina, J., and Ji, L.L. (2019). Intensified mitophagy in skeletal muscle with aging is downregulated by PGC-1alpha overexpression in vivo. Free Radic. Biol. Med. *130*, 361–368. https://doi.org/10.1016/j.freeradbiomed.2018.10.456.

22. Filadi, R., Pendin, D., and Pizzo, P. (2018). Mitofusin 2: from functions to disease. Cell Death Dis. *9*, 330. https://doi.org/10.1038/s41419-017-0023-6.

23. Arany, Z., Foo, S.-Y., Ma, Y., Ruas, J.L., Bommi-Reddy, A., Girnun, G., Cooper, M., Laznik, D., Chinsomboon, J., Rangwala, S.M., et al. (2008). HIF-independent regulation of VEGF and angiogenesis by the transcriptional coactivator PGC-1α. Nature *451*, 1008–1012. https://doi.org/10.1038/nature06613.

24. Arnold, A.-S., Gill, J., Christe, M., Ruiz, R., McGuirk, S., St-Pierre, J., Tabares, L., and Handschin, C. (2014). Morphological and functional remodelling of the neuromuscular junction by skeletal muscle PGC-1α. Nat. Commun. *5*, 3569. https://doi.org/10.1038/ncomms4569.

25. Selsby, J.T., Morine, K.J., Pendrak, K., Barton, E.R., and Sweeney, H.L. (2012). Rescue of dystrophic skeletal muscle by PGC-1α involves a fast to slow fiber type shift in the mdx mouse. PLoS One *7*, e30063. https://doi.org/10.1371/journal.pone.0030063.

26. Sandri, M., Lin, J., Handschin, C., Yang, W., Arany, Z.P., Lecker, S.H., Goldberg, A.L., and Spiegelman, B.M. (2006). PGC-1 protects skeletal muscle from atrophy by suppressing FoxO3 action and atrophy-specific gene transcription. Proc. Natl. Acad. Sci. *103*, 16260–16265. https://doi.org/10.1073/pnas.0607795103.

27. Handschin, C., Kobayashi, Y.M., Chin, S., Seale, P., Campbell, K.P., and Spiegelman, B.M. (2007). PGC-1 regulates the neuromuscular junction program and ameliorates Duchenne muscular dystrophy. Genes Dev. *21*, 770–783. https://doi.org/10.1101/gad.1525107.

28. Da Cruz, S., Parone, P.A., Lopes, V.S., Lillo, C., McAlonis-Downes, M., Lee, S.K., Vetto, A.P., Petrosyan, S., Marsala, M., Murphy, A.N., et al. (2012). Elevated PGC-1α activity sustains mitochondrial biogenesis and muscle function without extending survival in a mouse model of inherited ALS. Cell Metab *15*, 778–786. https://doi.org/10.1016/j.cmet.2012.03.019.

29. Cannavino, J., Brocca, L., Sandri, M., Bottinelli, R., and Pellegrino, M.A. (2014). PGC1-α over-expression prevents metabolic alterations and soleus muscle atrophy in hindlimb unloaded mice. J. Physiol. *592*, 4575–4589. https://doi.org/10.1113/jphysiol.2014.275545.

30. Cannavino, J., Brocca, L., Sandri, M., Grassi, B., Bottinelli, R., and Pellegrino, M.A. (2015). The role of alterations in mitochondrial dynamics and PGC-1α over-expression in fast muscle atrophy following hindlimb unloading. J. Physiol. *593*, 1981–1995. https://doi.org/10.1113/jphysiol.2014.286740.

31. Pin, F., Busquets, S., Toledo, M., Camperi, A., Lopez-Soriano, F.J., Costelli, P., Argilés, J.M., and Penna, F. (2015). Combination of exercise training and erythropoietin prevents cancer-induced muscle alterations. Oncotarget *6*, 43202–43215. https://doi.org/10.18632/oncotarget.6439.

32. Gill, J.F., Delezie, J., Santos, G., McGuirk, S., Schnyder, S., Frank, S., Rausch, M., St-Pierre, J., and Handschin, C. (2019). Peroxisome proliferator-activated receptor γ coactivator 1α regulates mitochondrial calcium homeostasis, sarcoplasmic reticulum stress, and cell death to mitigate skeletal muscle aging. Aging Cell *18*, e12993. https://doi.org/10.1111/acel.12993.

33. Schnyder, S., and Handschin, C. (2015). Skeletal muscle as an endocrine organ: PGC-1α, myokines and exercise. Bone *80*, 115–125. https://doi.org/10.1016/j.bone.2015.02.008.

34. Dinulovic, I., Furrer, R., Beer, M., Ferry, A., Cardel, B., and Handschin, C. (2016). Muscle PGC-1α modulates satellite cell number and proliferation by remodeling the stem cell niche. Skelet. Muscle *6*, 39. https://doi.org/10.1186/s13395-016-0111-9.

35. Furrer, R., Eisele, P.S., Schmidt, A., Beer, M., and Handschin, C. (2017). Paracrine cross-talk between skeletal muscle and macrophages in exercise by PGC-1α-controlled BNP. Sci. Rep. *7*, 40789. https://doi.org/10.1038/srep40789.

36. Dinulovic, I., Furrer, R., Di Fulvio, S., Ferry, A., Beer, M., and Handschin, C. (2016). PGC-1α modulates necrosis, inflammatory response, and fibrotic tissue formation in injured skeletal muscle. Skelet. Muscle *6*, 38. https://doi.org/10.1186/s13395-016-0110-x.

37. Duguez, S., Féasson, L., Denis, C., and Freyssenet, D. (2002). Mitochondrial biogenesis during skeletal muscle regeneration. Am. J. Physiol. Metab. *282*, E802–E809. https://doi.org/10.1152/ajpendo.00343.2001.

38. Sacco, A., Doyonnas, R., Kraft, P., Vitorovic, S., and Blau, H.M. (2008). Self-renewal and expansion of single transplanted muscle stem cells. Nature *456*, 502–506. https://doi.org/10.1038/nature07384.

39. Kopinke, D., Roberson, E.C., and Reiter, J.F. (2017). Ciliary hedgehog signaling restricts injury-induced adipogenesis. Cell *170*, 340–351.e12. https://doi.org/10.1016/j.cell.2017.06.035.

40. Schwalie, P.C., Dong, H., Zachara, M., Russeil, J., Alpern, D., Akchiche, N., Caprara, C., Sun, W., Schlaudraff, K.U., Soldati, G., et al. (2018). A stromal cell population that inhibits adipogenesis in mammalian fat depots. Nature *559*, 103–108. https://doi.org/10.1038/s41586-018-0226-8.

41. Merrick, D., Sakers, A., Irgebay, Z., Okada, C., Calvert, C., Morley, M.P., Percec, I., and Seale, P. (2019). Identification of a mesenchymal progenitor cell hierarchy in adipose tissue. Science *364*, eaav2501. https://doi.org/10.1126/science.aav2501.

42. Camps, J., Breuls, N., Sifrim, A., Giarratana, N., Corvelyn, M., Danti, L., Grosemans, H., Vanuytven, S., Thiry, I., Belicchi, M., et al. (2020). Interstitial cell remodeling promotes aberrant adipogenesis in dystrophic muscles. Cell Rep. *31*, 107597. https://doi.org/10.1016/j.celrep.2020.107597.

43. Pisani, D.F., Bottema, C.D.K., Butori, C., Dani, C., and Dechesne, C.A. (2010). Mouse model of skeletal muscle adiposity: a glycerol treatment approach. Biochem. Biophys. Res. Commun. *396*, 767–773. https://doi.org/10.1016/j.bbrc.2010.05.021.

44. Addison, O., Drummond, M.J., Lastayo, P.C., Dibble, L.E., Wende, A.R., McClain, D.A., and

Marcus, R.L. (2014). Intramuscular fat and inflammation differ in older adults: the impact of frailty and inactivity. J. Nutr. Health Aging *18*, 532–538. https://doi.org/10.1007/s12603-014-0019-1.

45. Sciorati, C., Clementi, E., Manfredi, A.A., and Rovere-Querini, P. (2015). Fat deposition and accumulation in the damaged and inflamed skeletal muscle: cellular and molecular players. Cell. Mol. Life Sci. *72*, 2135–2156. https://doi.org/10.1007/s00018-015-1857-7.

46. Shapira, S.N., and Christofk, H.R. (2020). Metabolic regulation of tissue stem cells. Trends Cell Biol. *30*, 566–576. https://doi.org/10.1016/j.tcb.2020.04.004.

47. Burgess, R.J., Agathocleous, M., and Morrison, S.J. (2014). Metabolic regulation of stem cell function. J. Intern. Med. *276*, 12–24. https://doi.org/10.1111/joim.12247.

48. Li, X., Egervari, G., Wang, Y., Berger, S.L., and Lu, Z. (2018). Regulation of chromatin and gene expression by metabolic enzymes and metabolites. Nat. Rev. Mol. Cell Biol. *19*, 563–578. https://doi.org/10.1038/s41580-018-0029-7.

49. Briggs, D., and Morgan, J.E. (2013). Recent progress in satellite cell/myoblast engraftment - relevance for therapy. FEBS J. *280*, 4281–4293. https://doi.org/10.1111/febs.12273.

50. Ganassi, M., Badodi, S., Wanders, K., Zammit, P.S., and Hughes, S.M. (2020). Myogenin is an essential regulator of adult myofibre growth and muscle stem cell homeostasis. Elife *9*, 1–23. https://doi.org/10.7554/eLife.60445.

51. Lukjanenko, L., Brachat, S., Pierrel, E., Lach-Trifilieff, E., and Feige, J.N. (2013). Genomic profiling reveals that transient adipogenic activation is a hallmark of mouse models of skeletal muscle regeneration. PLoS One *8*, e71084. https://doi.org/10.1371/journal.pone.0071084.

52. Boström, P., Wu, J., Jedrychowski, M.P., Korde, A., Ye, L., Lo, J.C., Rasbach, K.A., Boström, E.A., Choi, J.H., Long, J.Z., et al. (2012). A PGC1-α-dependent myokine that drives brown-fat-like development of white fat and thermogenesis. Nature *481*, 463–468. https://doi.org/10.1038/nature10777.

53. Sahu, A., Mamiya, H., Shinde, S.N., Cheikhi, A., Winter, L.L., Vo, N.V., Stolz, D., Roginskaya, V., Tang, W.Y., St. Croix, C., et al. (2018). Age-related declines in α-Klotho drive progenitor cell mitochondrial dysfunction and impaired muscle regeneration. Nat. Commun. *9*, 4859. https://doi.org/10.1038/s41467-018-07253-3.

54. Li, W., Zheng, Y., Zhang, W., Wang, Z., Xiao, J., and Yuan, Y. (2015). Progression and variation of fatty infiltration of the thigh muscles in Duchenne muscular dystrophy, a muscle magnetic resonance imaging study. Neuromuscul. Disord. *25*, 375–380. https://doi.org/10.1016/j.nmd.2015.01.003.

55. Hogarth, M.W., Defour, A., Lazarski, C., Gallardo, E., Diaz Manera, J., Partridge, T.A., Nagaraju, K., and Jaiswal, J.K. (2019). Fibroadipogenic progenitors are responsible for muscle loss in limb girdle muscular dystrophy 2B. Nat. Commun. *10*, 2430. https://doi.org/10.1038/s41467-019-10438-z.

56. Lin, J., Wu, H., Tarr, P.T., Zhang, C.-Y., Wu, Z., Boss, O., Michael, L.F., Puigserver, P., Isotani, E., Olson, E.N., et al. (2002). Transcriptional co-activator PGC-1α drives the formation of slow-twitch muscle fibres. Nature *418*, 797–801. https://doi.org/10.1038/nature00904.

57. Bergstrom, D.A., Penn, B.H., Strand, A., Perry, R.L.S., Rudnicki, M.A., and Tapscott, S.J. (2002). Promoter-specific regulation of MyoD binding and signal transduction cooperate to pattern gene expression. Mol. Cell *9*, 587–600. https://doi.org/10.1016/S1097-2765(02)00481-1.

58. Machado, L., Esteves de Lima, J., Fabre, O., Proux, C., Legendre, R., Szegedi, A., Varet, H., Ingerslev, L.R., Barrès, R., Relaix, F., et al. (2017). In situ fixation redefines quiescence and early activation of skeletal muscle stem cells. Cell Rep. *21*, 1982–1993. https://doi.org/10.1016/j.celrep.2017.10.080.

59. Sala, D., Cunningham, T.J., Stec, M.J., Etxaniz, U., Nicoletti, C., Dall'Agnese, A., Puri, P.L., Duester, G., Latella, L., and Sacco, A. (2019). The Stat3-Fam3a axis promotes muscle stem cell myogenic lineage progression by inducing mitochondrial respiration. Nat. Commun. *10*, 1796. https://doi.org/10.1038/s41467-019-09746-1.

60. Haralampieva, D., Salemi, S., Dinulovic, I., Sulser, T., Ametamey, S.M., Handschin, C., and Eberli, D. (2017). Human muscle precursor cells overexpressing PGC-1α enhance early skeletal muscle tissue formation. Cell Transplant. *26*, 1103–1114. https://doi.org/10.3727/096368917X694868.

STAR★METHODS

KEY RESOURCES TABLE

REAGENT or RESOURCE	SOURCE	IDENTIFIER
Antibodies		
Mouse monoclonal anti-α-Tubulin (clone B-5-1-2)	Sigma-Aldrich	Cat#T5168; RRID: AB_477579
Rat monoclonal anti-CD34 (clone RAM34), eFluor™ 450-conjugated	eBioscience	Cat#48-0341-82; RRID: AB_2043837
Armenian Hamster monoclonal anti-CD55 (clone RIKO-3), PE-conjugated	BioLegend	Cat#131803; RRID: AB_1279267
Rabbit monoclonal anti-CD142 (clone 001), APC-Vio770-conjugated	Sino Biological	Cat#50413-R001-P-50
Mouse monoclonal anti-COX-IV (clone 20E8C12)	Abcam	Cat#ab14744; RRID: AB_301443
Mouse monoclonal anti-GAPDH (clone GAPDH-71.1)	Sigma-Aldrich	Cat#G8795; RRID: AB_1078991
Mouse monoclonal anti-Integrin-α7 (clone 3C12), PE-Vio770-conjugated	Miltenyi Biotec	Cat#130-102-718; RRID: AB_2652468
Rabbit polyclonal anti-Laminin	Sigma-Aldrich	Cat#L9393; RRID: AB_477163
Mouse monoclonal anti-MyHC (clone MY-32)	Sigma-Aldrich	Cat#M4276; RRID: AB_477190
Mouse monoclonal anti-MyoG (clone F5D)	Santa Cruz Biotech	Cat#sc-12732; RRID: AB_627980
Mouse monoclonal anti-Pax7	DSHB	Cat#PAX7; RRID: AB_2299243
Rabbit polyclonal anti-Perilipin A/B	Sigma-Aldrich	Cat#P1873; RRID:AB_532267
Rabbit polyclonal anti-PGC-1α	Merck Millipore	Cat#AB3242; RRID: AB_2268462
Rat monoclonal anti-Sca1 (clone D7), APC-conjugated	eBioscience	Cat# 17-5981-82; RRID: AB_469487
Mouse monoclonal anti-SDHA (clone C-8)	Santa Cruz Biotech	Cat#sc-377302; RRID: AB_2904546
Goat anti-mouse IgG (H + L) Alexa Fluor™ 488	Invitrogen	Cat#A11001; RRID: AB_2534069
Goat anti-rabbit IgG (H + L) Alexa Fluor™ 488	Invitrogen	Cat#A11008; RRID: AB_143165
Goat anti-mouse IgG (H + L)-HRP Conjugate	Bio-Rad	Cat#170-6516; RRID: AB_11125547
Goat anti-rabbit IgG (H + L)-HRP Conjugate	Bio-Rad	Cat#170-6515; RRID: AB_11125142
Chemicals, peptides, and recombinant proteins		
Barium chloride ($BaCl_2$)	Sigma-Aldrich	Cat#202738
Collagenase/dispase	Roche Diagnostics	Cat#11097113001
Eosin Y disodium salt	Sigma-Aldrich	Cat#E4382
Eukitt Quick-hardening mounting medium	Sigma-Aldrich	Cat#03959
Hematoxylin	Sigma-Aldrich	Cat#51275
ECM gel (matrigel)	Sigma-Aldrich	Cat#E1270
Glycerol	Sigma-Aldrich	Cat#G9012
Igepal CA-630	Sigma-Aldrich	Cat#I3021
Nitrotetrazolium Blue chloride (NTB)	Sigma-Aldrich	Cat#N6876
Oil Red O (ORO)	Sigma-Aldrich	Cat#O0625
Pancreatine	Sigma-Aldrich	Cat#P3292
Phenol (pH 8.0)	Sigma-Aldrich	Cat#P4557
Phosphatase inhibitors	Sigma-Aldrich	Cat#P0044

(*Continued on next page*)

Continued

REAGENT or RESOURCE	SOURCE	IDENTIFIER
Quant-iT RiboGreen RNA Kit	Invitrogen	Cat#R11490
TRIReagent	Sigma-Aldrich	Cat#T9624
TWEEN20	Sigma-Aldrich	Cat#P1379
Type I collagenase	Sigma-Aldrich	Cat#C0130
Type II collagenase	Sigma-Aldrich	Cat#C6885
Critical commercial assays		
Satellite Cell Isolation Kit mouse	Miltenyi Biotec	Cat#130-104-268
cDNA synthesis kit	Bio-Rad	Cat#1708891
SsoAdvanced SYBR Green Supermix	Bio-Rad	Cat#1725274
Protein assay dye reagent	Bio-Rad	Cat#5000006
Deposited data		
Full uncropped WB bands	Mendeley Data	https://doi.org/10.17632/9w66cdzb3p.1
Experimental models: Cell lines		
Mouse: MuSCs isolated from skeletal muscle	This paper	N/A
Experimental models: Organisms/strains		
Mouse: Tg(Ckm-Ppargc1a)31Brsp/j (Balb/c)	This paper	N/A
Mouse: wild-type (Balb/c)	Charles River	N/A
Oligonucleotides		
Primers for RT-qPCR, see Table S2	This paper	N/A
Software and algorithms		
Axiovision 4.8.2	Zeiss	N/A
Bio-Rad CFX Maestro 1.0	Bio-Rad	N/A
BioRender	https://biorender.com/	N/A
GIMPShop	https://www.gimpshop.com/	N/A
GraphPad Prism v7	GraphPad Software	N/A
ImageJ	https://imagej.nih.gov/ij/	N/A
Image Lab	Bio-Rad	N/A

RESOURCE AVAILABILITY

Lead contact

Further information and requests for resources and reagents should be directed to and will be fulfilled by the lead contacts Fabio Penna (fabio.penna@unito.it) and Paola Costelli (paola.costelli@unito.it).

Material availability

The Tg(Ckm-Ppargc1a)31Brsp/j mouse line backcrossed to Balb/c strain is available upon request.

Data and code availability

Original western blot images have been deposited at the Mendeley Data repository. The DOI is listed in the key resources table. Western blotting densitometry and RT-qPCR data reported in this paper will be shared by the lead contact upon request.

This paper does not report original code.

Any additional information required to reanalyze the data reported in this paper is available from the lead contact upon request.

EXPERIMENTAL MODEL AND SUBJECT DETAILS

Animal housing and ethics

Experimental animals were cared for in compliance with the Italian Ministry of Health Guidelines and the Policy on Humane Care and Use of Laboratory Animals (NRC, 2011). The experimental protocols were approved by the Bioethical Committee of the University of Torino (Torino, Italy) and the Animal Welfare Committee of KU Leuven (Leuven, Belgium). Animals were maintained on a regular dark-light cycle of 12:12 h with controlled temperature (18-23°C) and free access to food and water during the whole experimental period.

Mouse models and experimental design

Balb/c mice overexpressing PGC-1α in the skeletal muscle (MCK-PGC-1α) were generated by backcrossing C57BL/6-Tg(Ckm-Ppargc1a)31Brsp/j mice[56] (The Jackson Laboratory, Bar Harbor, CA, USA) with WT Balb/c mice (Charles River, Wilmington, MA, USA). The resulting offspring was analyzed for the presence of the transgenic construct (forward: 5′-GCCGTGACCACTGCAACGA-3′ and reverse: 5′-CTGCATGGTTCTGA GTGCTAAG-3′) through Melt Curve Analysis (RT-qPCR) and selected for further crosses with WT Balb/c mice. The colony was maintained breeding mice as hemizygotes for 8 generations. During all intramuscular (i.m.) injections, the animals were anesthetized with 2% isoflurane in O2. The animals were sacrificed under anesthesia at specific time points. After intracardiac blood collection, euthanasia was applied by means of cervical dislocation. Skeletal muscles were excised, weighted, frozen in liquid nitrogen and stored at −80°C for further analyses.

The time course of muscle regeneration (animal experiment 1) was performed in WT 6-weeksold female mice receiving a local muscle injury (i.m. injection of 30 μL 1.2% $BaCl_2$) in the TA muscle. Contralateral TA muscles were injected with filtered 0.9% NaCl solution and used as controls (Saline). Animals were euthanized at 7, 10, 13 and 49 days dpi. Similarly, TA muscle injury of both WT and MCK-PGC-1α mice (animal experiment 2) was performed in 3-month and 12-monthsold female animals that were sacrificed at 14 dpi. Transplantation of isolated muscle-derived cells (animal experiment 3) was performed in WT 6-weeksold female mice previously injured in one of the TA muscles (approximately 8 h before cell injection, see Figure 3A). Injected cells were isolated from the hindlimb muscles of either WT or MCK-PGC-1α male mice according to an adaptation of the protocol described by Costamagna et al., 2020 (see below: *Whole muscle isolation, transplantation and flow cytometry analysis* section). Mice were euthanized at 14 dpi. As for adipogenesis study, Gly injury (animal experiment 4) was performed by i.m. injection of 30 μL 50% glycerol (G9012, Sigma-Aldrich) sterile solution in the TA muscles of WT and MCK-PGC-1α 3-monthsold female mice. Animals were euthanized 21 dpi.

Organ culture

EDL and *Soleus* muscles from 6-weeksold male mice (WT and MCK-PGC-1α) were rapidly excised, rinsed in sterile PBS containing 5% antibiotics (9:1 penicillin/streptomycin:gentamicin) and digested in PBS containing 0.02% type I collagenase (C0130, Sigma-Aldrich, Burlington, MA, USA) for 1 h at 37°C. Digested muscles were plated on matrigel-coated dishes in DMEM high glucose (D6429, Sigma-Aldrich) supplemented with 20% fetal bovine serum (FBS), 10% horse serum, 0.5% chicken embryo extract and 1% penicillin-streptomycin. Three days later, muscle remnant was removed and medium was replaced with proliferation medium (DMEM high glucose, 20% FBS, 10% horse serum, 1% chicken embryo extract). After 5 days, the medium was replaced with differentiation medium (DMEM high glucose, 2% horse serum and 0.5% chicken embryo extract).

MuSCs isolation, culture and differentiation

Cultured MuSCs were isolated using two sequential enzymatic digestions while shaking at 37°C: a first incubation with 0.04% collagenase II for 45 min, followed by 30 min digestion with 0.1% collagenase/dispase (11,097,113,001, Roche Diagnostics, Mannheim, Germany). MuSCs were selected using the Satellite Cell Isolation Kit mouse (130-104-268, Miltenyi Biotec, Bergisch Gladbach, Germany), seeded at 2 000 cells/cm^2 and grown for 3 days in growth medium containing 20% horse serum, 3% chicken embryo extract, 1% HEPES, 1% glutamine and 1% penicillin-streptomycin. To induce myotube formation, GM was replaced with differentiating medium containing 2% horse serum and kept for 3 days.

METHOD DETAILS

Myosin quantification

Primary myotubes generated from organ cultures were washed with PBS and fixed in acetone-methanol solution (1:1). Samples were then probed with anti-MyHC antibody (1/100, M4276, Sigma-Aldrich) followed by labeling with an Alexa488-conjugated secondary antibody (1/1000; Invitrogen, Carlsbad, CA, USA) and nuclei were counterstained with Hoechst 33,342. Subsequently, myotubes were lysed with RIPA buffer (50 mM Tris-HCl pH 7.4, 150 mM NaCl, 1% Igepal CA-630 (I3021, Sigma-Aldrich), 0.25% sodium deoxycholate, 1 mM PMSF), sonicated and centrifuged at 3000 rpm for 5 min. The pellet was discarded and fluorescence intensity of the supernatant was assessed (Alexa488: ~495 nm excitation, ~519 nm emission; Hoechst 33,342: ~358 nm excitation, ~461 nm emission).

Whole muscle cell isolation, transplantation and flow cytometric analysis

Hindlimb muscles from 6-weeksold male mice (WT and MCK-PGC-1α) were mechanically minced using a scalpel, washed with 5% antibiotics and enzymatically digested with 0.02% type I collagenase and 0.06% pancreatine (P3292, Sigma-Aldrich) upon shaking for 1 h at 37°C. The suspension was then filtered using 70 μm strainers, the digestion was blocked with fetal bovine serum and cell suspension was kept at 37°C while the solid part was re-digested for additional 30 min repeating the steps above. For cell transplantation, the cell suspension was centrifuged for 5 min at 400*g* at room temperature, resuspended in sterile saline solution and the equivalent amount of cells obtained from one TA donor muscle was injected in either injured or intact TA muscle of WT recipient mice. As for flow cytometric analysis, hindlimb muscles were enzymatically digested with 0.1% type II collagenase (C6885, Sigma-Aldrich). Isolated cells were resuspended in growing medium (DMEM high glucose with 10% FBS) and kept at 37°C. After 4 h, samples (100,000 cells) were probed with different combinations of conjugated primary antibodies (Table S1) and analyzed by flow cytometry (Canto II AIG, BD Biosciences, Franklin Lakes, NJ, USA). Cell debris, dead cells and cell doublets were excluded based on scatter signals (Figure S2E). Fluorescence minus one (FMO) controls were used to establish gating boundaries of antibody-specific signal. Absolute quantification of specific cell populations was calculated by normalizing relative quantification with the total number of cells isolated per mass of muscle tissue (data reported in Figure 2B).

Muscle histology

TA muscles were frozen in melting isopentane cooled in liquid nitrogen and stored at −80°C. Transverse sections of 10 μm from the midbelly region were cut on a cryostat, left at room temperature for 10 min and stored at −80°C for later staining. Hematoxylin/eosin staining (H&E) was performed following standard procedures. SDH staining was performed by incubating pre-warmed sections with SDH reagent (1 mg/mL NTB, 27 mg/mL sodium succinate in PBS) at 37°C for 20 min. Slides were then rinsed twice with PBS, dehydrated using ethanol scale and xylene, mounted using Eukitt Quick-hardening mounting medium (03,959, Sigma-Aldrich). ORO staining was performed on sections fixed with 4% paraformaldehyde by incubating Oil Red O solution (0.5% in propylene glycol) at 60°C for 15 min. After washing with 85% propylene glycol for 5 min, slides were counterstained with hematoxylin for 1 min, air-dried and mounted with glycerol-PBS (3:1). Images were captured by a Leica DM750 optical microscope (Leica Camera AG, Wetzlar, Germany).

For immunofluorescence, the sections were fixed in 4% paraformaldehyde for 15 min, rinsed in PBS and probed with primary anti-Laminin (1/100, L9393, Sigma-Aldrich) or anti-Perilipin A/B (½00, P1873, Sigma-Aldrich) antibodies. Detection was performed with Alexa488-conjugated secondary antibody (1/1000; Invitrogen) and nuclei were counterstained with Hoechst 33,342. Slides were mounted with glycerol-PBS (3:1) and fluorescence images were captured by an Axiovert 35 fluorescence microscope (Zeiss, Oberkochen, Germany) without altering light exposure parameters. Whole muscle sections were generated using the GIMPShop software. Quantification of central nuclei and perilipin densitometry were performed on whole TA muscle sections using the ImageJ software.

Isolation, retro-transcription and RT-qPCR quantification of mRNA

TA muscles were lysed in 1 mL of TRIReagent (T9624, Sigma-Aldrich) and processed using the standard phenol-chloroform method. Briefly, 50 μm thick muscle sections were shaken in 1 mL of TRIReagent for 30 min at 4°C, added 200 μL chloroform, mixed vigorously and centrifuged at 12,000 *g* for 15 min. The RNA in the aqueous part was precipitated by 2-propanol and 70% ethanol, dried at room temperature

and resuspended in sterile water. RNA concentration was quantified using the Ribogreen reagent (R11490, Invitrogen). Total RNA was retro-transcribed using cDNA synthesis kit (1,708,891, Bio-Rad, Hercules, CA, USA) and transcript levels were determined by RT-qPCR using the SsoAdvanced SYBR Green Supermix (1,725,274, Bio-Rad) and the CFX Connect Real-Time PCR Detection System (Bio-Rad). Every RT-qPCR was validated by analyzing the respective melting curve. Primer sequences are given in Table S2. Gene expression was normalized to *Actb* (muscle tissue) or *H2bc4* (cells) and results are expressed as relative expression ($2^{-\Delta\Delta Ct}$).

Quantification of mtDNA

Approximately 20mg of *Gastrocnemius* muscle were incubated in 0.5 mL DNA digestion buffer (50 mM Tris-HCl pH 8.0, 100 mM EDTA pH 8.0, 100 mM NaCl, 1% SDS) overnight at 50°C with gentle shaking. Next, 0.7 mL of a mixture of neutralized phenol (pH 8.0; P4557, Sigma-Aldrich), chloroform and isoamyl alcohol (25:24:1) was added and mixed for 1 h using a cylindrical rotor. Tubes were then centrifuged at 12,000 *g* for 5 min and the DNA contained in the aqueous phase was precipitated using 1 mL of ethanol, centrifuged and washed with cold 70% ethanol. DNA was then pelleted by centrifugation at 12,000*g* for 5 min at 4°C, resuspended in 100 µL of sterile water and quantified spectrophotometrically. The relative amount of mtDNA was determined by RT-qPCR as the geometric mean of rRNA 16s and cytochrome *c* oxidase subunit II (Cox2) genes (mitochondrial genome) and normalized to the geometric mean of uncoupling protein 2 (Ucp2) and hexokinase-2 (Hk2) genes (nuclear genome). Primer sequences are listed in Table S2.

Western blotting

TA muscles were mechanically homogenized in RIPA buffer (50 mM Tris-HCl pH 8.0, 5 mM EDTA pH 8.0, 1% Igepal CA-630, 0.5% sodium deoxycholate 0.1% SDS) containing protease inhibitors (0.5 mM PMSF, 0.5 mM DTT, 2 µg/mL leupeptin, 2 µg/mL aprotinin) and phosphatase inhibitors (P0044, Sigma-Aldrich), sonicated for 10 s at low intensity, centrifuged at 15,000 *g* for 5 min at 4°C and the supernatant was collected. Total protein concentration was quantified with the Protein assay dye reagent (5,000,006, Bio-Rad), using BSA as protein concentration standard. Equal amounts of protein (15-30 µg) were heat-denatured in sample-loading buffer (50 mM Tris-HCl pH 6.8, 100 mM DTT, 2% SDS, 0.1% bromophenol blue, 10% glycerol), resolved by SDS-PAGE and transferred to nitrocellulose membranes (Bio-Rad). The filters were blocked with Tris-buffered saline containing 0.05% Tween and 5% non-fat dry milk and then incubated overnight with antibodies directed against specific proteins: α-Tubulin (1/1000; T5168, Sigma-Aldrich), COX-IV (1/1000; ab14744, Abcam), GAPDH (1/10,000; G8795, Sigma-Aldrich), MyoG (1/500; sc-12732, Santa Cruz Biotech), Pax7 (½0; DSHB), PGC-1α (1/1000; AB3242, Merck Millipore) and SDHA (1/500; sc-377302, Santa Cruz Biotech). Goat anti-mouse or goat anti-rabbit HRP-conjugated IgGs (Bio-Rad) were used as secondary antibodies and chemiluminescent signal was captured using either Hyperfilm ECL films (GE28-9068-36, Cytiva, United Kingdom) or the ChemiDoc XRS+ imaging system (Bio-Rad). Quantification of the bands was performed by densitometric analysis using the Image Lab software (Bio-Rad).

QUANTIFICATION AND STATISTICAL ANALYSIS

Data are presented using bar plots (mean) with individual values unless differently stated. Data representation and evaluation of statistical significance was performed with Prism (version 7, GraphPad) software. Normal distribution was evaluated by Shapiro-Wilk test. The significance of the differences was evaluated by appropriate two-sided statistical tests, being Student's "t"-test or ANOVA for normal distribution, and Mann–Whitney test or Kruskal–Wallis test for nonnormal distribution. ANOVA and Kruskal–Wallis tests were followed by suitable post hoc analysis as stated in figure legends. A pvalue (*P*) of <0.05 was considered statistically significant. The details of the statistical analysis used in each experiment are found in the figure legends.